Bulk Superconductivity Induced by Se Substitution in BiCh$_2$-Based Layered Compounds Eu$_{0.5}$Ce$_{0.5}$FBiS$_{2-x}$Se$_x$

Yosuke Goto, Ryota Sogabe, and Yoshikazu Mizuguchi*

Department of Physics, Tokyo Metropolitan University, Hachioji 192-0397, Japan

*E-mail: mizugu@tmu.ac.jp

Abstract

We report the effect of Se substitution on the crystal structure and superconductivity of BiCh$_2$-based (Ch: S, Se) layered compounds Eu$_{0.5}$Ce$_{0.5}$FBiS$_{2-x}$Se$_x$ (x = 0–1). Crystal structure analysis showed that both lattice constants, a and c, increased with increasing x, which is different from the related La-doped system, such as Eu$_{0.5}$La$_{0.5}$FBiS$_{2-x}$Se$_x$. This is due to Se substitution for both in-plane and out-of-plane Ch sites in the present Ce-doped system. Zero resistivity was observed for x = 0.2–1 above 2 K. Superconducting properties of Eu$_{0.5}$Ce$_{0.5}$FBiS$_{2-x}$Se$_x$ was investigated by magnetic susceptibility, and the highest superconducting transition temperature of 3.5 K was obtained for x = 0.6 with a large shielding volume fraction. The emergence of bulk superconductivity and metallic conductivity can be qualitatively described in terms of increased in-plane chemical pressure effect. A magnetic anomaly below 8 K, probably because of ferromagnetic order of magnetic moment of Ce^{3+} ions, coexists with bulk superconductivity in BiCh$_2$ layer. Since the effect of Se substitution on the magnetic transition temperature is ignorable, we suggest that the coupling between the magnetic order at the (Eu,Ce)F layer and superconductivity at the Bi(S,Se)$_2$ layer is weak.

Introduction

There has been considerable interest in the study of $BiCh_2$-based (Ch: S, Se) layered compounds because of their unique functionalities including superconductivity, thermoelectricity, and so forth [1]. The layered crystal structure of the $BiCh_2$-based system consists of conducting $BiCh_2$ layers alternating with electrically insulating (blocking) layers, which resembles those of cuprate or Fe-based high-transition-temperature (T_c) superconductors [2,3]. Since the discovery of superconductivity in $Bi_4O_4S_3$ and $REO_{1-x}F_xBiS_2$ (RE: rare-earth element), several types of $BiCh_2$-based superconductors have been reported [1,4,5]. Although many experimental and theoretical studies have been devoted to clarify the superconductivity mechanism and to increase the T_c of the $BiCh_2$-based superconductors, the consensus on the nature of superconductivity is yet to be achieved. Furthermore, recent measurements of laser-based angle-resolved photoemission spectroscopy [6] and first-principles calculations [7] have demonstrated that weak-coupling electron-phonon mechanism cannot describe the emerging T_c of the $BiCh_2$-based superconductors. Therefore, systematic characterization is still crucial to clarify the superconductivity mechanism of these compounds.

As an example, $LaOBiS_2$ is a semiconductor with a band gap value of 1 eV, and superconductivity is induced by F^--substitution for O^{2-}. This result suggests the conventional scenario that the emergence of superconductivity owing to electron carrier doping into the conduction band consisting of hybridized Bi 6p and Ch p orbitals [8,9]. Although electron carrier doping is believed to be essential to induce superconductivity in $BiCh_2$-based compounds, optimally doped $LaO_{0.5}F_{0.5}BiS_2$ only shows weak (filamentary) superconductivity rather than bulk superconductivity. To induce bulk superconductivity in this system, external pressure effects [10–17] and/or element substitution at the La or S sites [18–21], are available. These characteristics have been qualitatively described by sufficient orbital overlapping between in-plane Bi and Ch as a results of in-plane chemical pressure effect [22]. Indeed, it has been reported that such pressure effects successfully suppressed the in-plane disorder of $BiCh_2$ conducting layer, which was demonstrated by means of synchrotron X-ray diffraction, extended X-ray absorption fine structure, and neutron diffraction [22–26]. The typical example is the $Eu_{0.5}La_{0.5}FBiS_{2-x}Se_x$ system [27]. $Eu_{0.5}La_{0.5}FBiS_2$, whose carrier concentration corresponds to 0.5 electron doping per Bi atoms as in the case of $LaO_{0.5}F_{0.5}BiS_2$, does not show bulk superconductivity, while the superconductivity is induced by Se substitution owing to the increased in-plane chemical pressure effect.

In the present study, we report the synthesis, crystal structure analyses, and superconducting properties of $Eu_{0.5}Ce_{0.5}FBiS_{2-x}Se_x$. It has been reported that

$Eu_{0.5}Ce_{0.5}FBiS_2$ showed the coexistence of superconductivity and magnetic order of RE moment [28]. However, bulk superconductivity has yet been achieved for the compound. We have demonstrated Se substitution successfully induced bulk superconductivity in $Eu_{0.5}Ce_{0.5}FBiS_{2-x}Se_x$, which was qualitatively described by an increase of in-plane chemical pressure, as the case of La-doped $Eu_{0.5}La_{0.5}FBiS_{2-x}Se_x$. Although magnetic order due to the Ce^{3+} moment coexisted with superconductivity in $BiCh_2$ layer, it was suggested that coupling between them was ignorable.

Experiments

Polycrystalline samples of $Eu_{0.5}Ce_{0.5}FBiS_{2-x}Se_x$ with $x = 0$, 0.2, 0.4, 0.6, 0.8, and 1 were prepared by solid-state reaction of EuS (99.9%), Ce_2S_3 (99.9%), BiF_3 (99.9%), Bi (99.999%), S (99.99%), and Se (99.999%). Stoichiometric mixtures of these starting materials were pressed into pellets and sealed in a sealed quartz tube. The heating temperature was optimized for each composition: the samples were heated for 20 h at 780 °C for $x = 0$, at 700 °C for $x = 0.2$ and 0.4, at 650 °C for $x = 0.6$ and 0.8, and at 600 °C for $x = 1$. The obtained product was ground, mixed, pelletized, and heated again under the same heating condition.

The obtained samples were characterized using powder X-ray diffraction (XRD) using a CuKα radiation (Rigaku, Miniflex 600 equipped with a D/teX Ultra detector). The XRD patterns were analyzed using the Rietveld method using RIETAN-FP code [29]. Crystal structure was depicted using VESTA software [30]. Magnetic susceptibility (χ) as a function of temperature (T) was measured using a superconducting quantum interference device (SQUID) magnetometer (Quantum Design, MPMS-3) with an applied field of 5 Oe after both zero-field cooling (ZFC) and field cooling (FC). The T dependence of electrical resistivity (ρ) was measured using a four-terminal method.

Results and Discussion

Figure 1(a) shows the XRD patterns of $Eu_{0.5}Ce_{0.5}FBiS_{2-x}Se_x$ ($x = 0-1$). Almost all of diffraction peaks are assigned to those of $EuFBiS_2$-type tetragonal phase, indicating that the obtained samples are nearly single-phase. Several diffraction peaks due to impurity phase such as Bi_2Se_3 were also observed, as indicated by the asterisks in the Figure 1(a). However, both of lattice constants a and c increase with increasing x, as shown in Figure 1(b), indicating Se ions are successfully and systematically substituted for S ions in $Eu_{0.5}Ce_{0.5}FBiS_{2-x}Se_x$. Notably, linear relationships between lattice constants and Se content were observed, which were different from the related La-doped systems, such as $Eu_{0.5}La_{0.5}FBiS_{2-x}Se_x$, where a increases with increasing x, but c does not show apparent

changes with increasing x [22]. These characteristics were most likely due to site selectivity of Se substitution. In the case of $Eu_{0.5}La_{0.5}FBiS_{2-x}Se_x$, Se ions selectively occupy in-plane Ch1 site rather than out-of-plane Ch2 site, where schematic representation of crystal structure was shown in Figure 1(c). Such selective substitution for Ch site resulted in anisotropic elongation of lattice constants of $Eu_{0.5}La_{0.5}FBiS_{2-x}Se_x$. On the other hand, as shown in Figure 2, substituted Se ions occupy both of the Ch sites (Ch1 and Ch2) for $Eu_{0.5}Ce_{0.5}FBiS_{2-x}Se_x$, resulting in increases of both a and c with increasing x. Figures 3(a)–(d) show the in-plane Bi–Ch1 distance, inter-plane Bi–Ch1 bond distance, Bi–Ch2 bond distance, and RE–Ch2 distance. These bond distances seem to be correlating with the lattice constants a and c. For example, Bi–Ch1 and RE–Ch2 distance tend to increase with increasing x. Besides, Bi–Ch2 distance and inter-plane Bi–Ch1 distance seem to be decreased as a result of Se-substitution. Such shrinkage is different from the crystal structure evolution of $Eu_{0.5}La_{0.5}FBiS_{2-x}Se_x$ by Se substitution [31].

As previously demonstrated, the in-plane chemical pressure (CP) of $BiCh_2$-based layered compounds can be qualitatively described with the following equation: $CP = (R_{Bi} + R_{Ch1})/$(Bi–Ch1 bond distance), where R_{Bi} is obtained from the average Bi–S bond distance for $LaO_{0.54}F_{0.46}BiS_2$ [22]. The Bi–Ch1 bond distance was calculated using the results of the Rietveld refinement. Figure 4 shows the in-plane CP as a function of x for $Eu_{0.5}Ce_{0.5}FBiS_{2-x}Se_x$. The CP monotonically increase with increasing x, indicating orbital overlap between Bi and Ch is enhanced by Se substitution. However, the value is lower than that of La-substituted systems $Eu_{0.5}La_{0.5}OBiS_{2-x}Se_x$ [27]. This is because of indistinct site selectivity of Se substitution in $Eu_{0.5}Ce_{0.5}FBiS_{2-x}Se_x$, as described above.

Figure 4(a) shows χ–T plots with an applied magnetic field of 5 Oe after ZFC for $Eu_{0.5}Ce_{0.5}FBiS_{2-x}Se_x$. Clear diamagnetic signals were not obtained for $x = 0$. Besides, diamagnetic signals corresponding to the emergence of superconductivity were observed for $x \geq 0.2$. The largest shielding volume fraction and T_c of 3.5 K were obtained for $x = 0.6$, as shown in Figure 4(b), indicating that this is a bulk superconductor. The large shielding fraction exceeding $-1/4\pi$ should be due to demagnetization effect for the polycrystalline sample containing many plate crystals. For $x = 0$, a gradual increase of χ was observed below 8 K. It has been reported that magnetic moment of Ce^{3+} ions of $CeO_{0.3}F_{0.7}BiS_2$ aligned ferromagnetically, which was demonstrated using neutron scattering measurements [32]. Therefore, the increase of χ below 8 K in the present sample would be attributable to the ferromagnetic ordering of Ce^{3+} moment, as well. It is interesting to note that the amplitude of the magnetic transition was suppressed for $x = 0.2$ and 0.4, and was emerged again for $x \geq 0.6$, as shown in Figure S2. Although

superconductivity was suppressed with increasing x for $x > 0.6$, the magnetic transition was almost unchanged in this region. In addition, the magnetic transition temperature never changes with x, while superconducting T_c clearly depends on x. These results suggest that the coupling between superconductivity at the $BiCh_2$ layer and the magnetic order at the $Eu_{0.5}Ce_{0.5}F$ layer is notably weak. At present, we have no idea to explain the suppression of the amplitude of the magnetic transition for $x = 0.2$ and 0.4. However, the valence states of Eu and Ce in $Eu_{0.5}Ce_{0.5}FBiS_{2-x}Se_x$ would be essentially sensitive to its chemical composition and/or crystal structure, as recently reported in $Eu_{0.5}La_{0.5}FBiS_{2-x}Se_x$ [33]. In addition, X-ray absorption spectroscopy revealed that mixed valence of Ce ions was suppressed by F doping for $CeO_{1-x}F_xBiS_2$ [34,35]. It was suggested that Ce-S-Bi coupling channel is essential to drive the system from the valence fluctuation regime to the Kondo-like regime. Further investigation of local crystal/electronic structure is required to clarify the detailed relationship between magnetism and superconductivity in $Eu_{0.5}Ce_{0.5}FBiS_{2-x}Se_x$.

Figure 5 shows ρ as a function of T. For $x \leq 0.4$, $\rho-T$ plots shows semiconducting-like behavior, that is, ρ increases with decreasing T. This semiconducting-like T dependence is probably due to localization of doped electrons. Metallic-like $\rho-T$ characteristics were observed for $x \geq 0.6$. Note that carrier concentration is believed to be almost identical in $Eu_{0.5}Ce_{0.5}FBiS_{2-x}Se_x$ because of isovalent substitution of S^{2-} with Se^{2-} ions [36]. However, metallic-like $\rho-T$ plots were induced by Se substitution owing to an increase of in-plane CP, as in the case of $Eu_{0.5}La_{0.5}FBiS_{2-x}Se_x$ [27].

On the superconducting characteristics, the onset of the superconducting transition was evaluated to be $T_c^{onset} = 2.3$ K for $x = 0$, although zero resistivity was not obtained down to 1.9 K, as shown in Figure 5(b). Besides, zero resistivity was observed for $x \geq 0.2$, which is consistent with a diamagnetic signal of $\chi-T$ plots. The T_c^{zero} of 3.5 K was obtained for $x = 0.6-1$, as shown in Figure 5(c), and it was also consistent with T_c estimated from $\chi-T$ plots. Notably, ρ gradually decreases well above T_c^{zero} : T_c^{onset} can be estimated to be 5.4 K for $x = 0.6$. Such a gradual decrease of ρ is probably because of a local evolution of superconductivity with a higher T_c, as demonstrated in $NdO_{1-x}F_xBi_{1-y}S_2$ single crystals [37].

A superconductivity phase diagram established using $\chi-T$ and $\rho-T$ plots are depicted in Fig. 7. The semiconducting-like $\rho-T$ behavior and filamentary weak superconducting transition with T_c^{onset} of 2.3 K was observed $x = 0$. The semiconducting-like behavior was suppressed by Se substitution, and bulk superconductivity with a large shielding volume fraction was observed. The highest T_c was 3.5 K for $x = 0.6$. Evidently, the superconducting properties of $Eu_{0.5}La_{0.5}OBiS_{2-x}Se_x$ was optimized for $x = 0.6$, at the

5

boundary of semiconducting-metallic phase transition. Such emergence of metallic-like ρ–T behavior and bulk superconductivity was quite similar to the case of related compounds, such as $Eu_{0.5}La_{0.5}FBiS_{2-x}Se_x$ [27]. Thus, the importance of the in-plane CP for the emergence of metallic conductivity and bulk superconductivity in $BiCh_2$-based compounds are clearly shown with the new $BiCh_2$-based superconductor system.

Conclusions

We have synthesized a new $BiCh_2$-based superconductor system, $Eu_{0.5}Ce_{0.5}FBiS_{2-x}Se_x$. Polycrystalline samples for $x = 0$–1 were prepared by a solid-state reaction. Both lattice constants, a and c, monotonically increases with increasing x. This linear relationship between lattice constants and Se content is different from that of related compounds, such as $Eu_{0.5}La_{0.5}FBiS_{2-x}Se_x$. Crystal structure analysis by the Rietveld refinement showed that this is due to the indistinct site selectivity of Se substitution; namely, Se occupied both of in-plane Ch1 and out-of-plane Ch2 sites. The sample with $x = 0$ exhibited the semiconducting-like ρ–T and weak superconducting signals. Metallic-like conductivity and bulk superconductivity were induced by Se substitution. Such characteristics were qualitatively described in terms of increased in-plane CP, as in the case of related compounds. The highest T_c was 3.5 K for $x = 0.6$, and superconductivity phase diagram was established. Magnetic transition, probably due to ferromagnetic order of magnetic moment of Ce^{3+}, coexists with bulk superconductivity in $BiCh_2$ layer. The coupling between superconductivity and magnetic order is ignorable in $Eu_{0.5}Ce_{0.5}FBiS_{2-x}Se_x$.

References

1) Y. Mizuguchi, Chem. Rec. **16**, 633 (2016).

2) J. B. Bednorz and K. Müller, Z. Phys. B **64**, 189 (1986).

3) Y. Kamihara, T. Watanabe, M. Hirano, and H. Hosono, J. Am. Chem. Soc. 130, 3296 (2008).

4) Y. Mizuguchi, H. Fujihisa, Y. Gotoh, K. Suzuki, H. Usui, K. Kuroki, S. Demura, Y. Takano, H. Izawa, and O. Miura, Phys. Rev. B 86, 220510 (2012).

5) Y. Mizuguchi, S. Demura, K. Deguchi, Y. Takano, H. Fujihisa, Y. Gotoh, H. Izawa, and O. Miura, J. Phys. Soc. Jpn. 81, 114725 (2012).

6) Y. Ota, K. Okazaki, H. Q. Yamamoto, T. Yamamoto, S. Watanabe, C. Chen, M. Nagao, S. Watauchi, I. Tanaka, Y. Takano, and S. Shin, Phys. Rev. Lett. 118, 167002 (2017).

7) C. Morice, R. Akashi, T. Koretsune, S. S. Saxena, and R. Arita, Phys. Rev. B 95, 180505 (2017).

8) H. Usui, K. Suzuki, and K. Kuroki, Phys. Rev. B 86, 220501(R) (2012).

9) H. Usui and K. Kuroki, Novel Supercond. Mater. 1, 50 (2015).

10) R. Jha, H. Kishan, and V. P. S. Awana, J. Phys. Chem. Solids 84, 17 (2015).

11) T. Tomita, M. Ebata, H. Soeda, H. Takahashi, H. Fujihisa, Y. Gotoh, Y. Mizuguchi, H. Izawa, O. Miura, S. Demura, K. Deguchi, and Y. Takano, J. Phys. Soc. Jpn. 83, 063704 (2014).

12) C. T. Wolowiec, D. Yazici, B. D. White, K. Huang and M. B. Maple, Phys. Rev. B 88, 064503 (2013).

13) C. T. Wolowiec, B. D. White, I. Jeon, D. Yazici, K. Huang, and M. B. Maple, J. Phys.: Condens. Matter 25, 422201 (2013).

14) K. Deguchi, Y. Mizuguchi, S. Demura, H. Hara, T. Watanabe, S. J. Denholme, M. Fujioka, H. Okazaki, T. Ozaki, H. Takeya, T. Yamaguchi, O. Miura, and Y. Takano, EPL 101, 17004 (2013).

15) J. Kajitani, K. Deguchi, A. Omachi, T. Hiroi, Y. Takano, H. Takatsu, H. Kadowaki, O. Miura, and Y. Mizuguchi, Solid State Commun. 181, 1 (2014).

16) J. Kajitani, K. Deguchi, T. Hiroi, A. Omachi, S. Demura, Y. Takano, O. Miura, and Y. Mizuguchi, J. Phys. Soc. Jpn. 83, 065002 (2014).

17) S. Demura, Y. Mizuguchi, K. Deguchi, H. Okazaki, H. Hara, T. Watanabe, S. J. Denholme, M. Fujioka, T. Ozaki, H. Fujihisa, Y. Gotoh, O. Miura, T. Yamaguchi, H. Takeya, and Y. Takano, J. Phys. Soc. Jpn. 82, 033708 (2013).

18) D. Yazici, K. Huang, B. D. White, A. H. Chang, A. J. Friedman, and M. B. Maple, Philosophical Magazine 93, 673 (2012).

19) R. Jha, A. Kumar, S. K. Singh, and V. P. S. Awana, J. Appl. Phys. 113, 056102 (2013).

20) S. Demura, K. Deguchi, Y. Mizuguchi, K. Sato, R. Honjyo, A. Yamashita, T. Yamaki, H. Hara, T. Watanabe, S. J. Denholme, M. Fujioka, H. Okazaki, T. Ozaki, O. Miura, T. Yamaguchi, H. Takeya, and Y. Takano, J. Phys. Soc. Jpn. 84, 024709 (2015).

21) S. Demura, Nov. Supercond. Mater. 2, 1 (2016).

22) Y. Mizuguchi, A. Miura, J. Kajitani, T. Hiroi, O. Miura, K. Tadanaga, N. Kumada, E. Magome, C. Moriyoshi, and Y. Kuroiwa, Sci. Rep. 5, 14968 (2015).

23) E. Paris, B. Joseph, A. Iadecola, T. Sugimoto, L. Olivi, S. Demura, Y. Mizuguchi, Y. Takano, T. Mizokawa, and N. L. Saini, J. Phys.: Condens. Matter 26, 435701 (2014).

24) Y. Mizuguchi, E. Paris, T. Sugimoto, A. Iadecola, J. Kajitani, O. Miura, T. Mizokawa, and N. L. Saini, Phys. Chem. Chem. Phys. 17, 22090 (2015).

25) A. Athauda, J. Yang, S. Lee, Y. Mizuguchi, K. Deguchi, Y. Takano, O. Miura, and D. Louca, Phys. Rev. B 91, 144112 (2014).

26) K. Nagasaka, A. Nishida, R. Jha, J. Kajitani, O. Miura, R. Higashinaka, T. D. Matsuda, Y. Aoki, A. Miura, C. Moriyoshi, Y. Kuroiwa, H. Usui, K. Kuroki, and Y. Mizuguchi, J. Phys. Soc. Jpn. 86, 074701 (2017).

27) G. Jinno, R. Jha, A. Yamada, R. Higashinaka, T. D. Matsuda, Y. Aoki, M. Nagao, O. Miura, and Y. Mizuguchi, J. Phys. Soc. Jpn. **85**, 2 (2016).

28) H. Zhai, P. Zhang, Z. Tang, J. Bao, H. Jiang, C. Feng, Z. Xu, and G. Cao, J. Phys. Condens. Matter **27**, 385701 (2015).

29) F. Izumi and K. Momma, Solid State Phenom. 130, 15 (2007).

30) K. Momma and F. Izumi, J. Appl. Crystallogr. 41, 653 (2008).

31) K. Nagasaka, G. Jinno, O. Miura, A. Miura, C. Moriyoshi, Y. Kuroiwa, and Y. Mizuguchi, J. Phys. Conf. Ser. **871**, 12007 (2017).

32) J. Lee, S. Demura, M. B. Stone, K. Iida, G. Ehlers, C. R. Cruz, M. Matsuda, K. Deguchi, Y. Takano, Y. Mizuguchi, O. Miura, D. Louca, and S. Lee, Phys. Rev. B **90**, 224410 (2014).

33) Y. Mizuguchi, E. Paris, T. Wakita, G. Jinno, A. Puri, K. Terashima, B. Joseph, O. Miura, T. Yokoya, and N. L. Saini, Phys. Rev. B 95, 064515 (2017).

34) T. Sugimoto, B. Joseph, E. Paris, A. Iadecola, T. Mizokawa, S. Demura, Y. Mizuguchi, Y. Takano, and N. L. Saini, Phys. Rev. B **89**, 201117(R) (2014).

35) T. Sugimoto, D. Ootsuki, E. Paris, A. Iadecola, M. Salome, E. F. Schwier, H. Iwasawa, K. Shimada, T. Asano, R. Higashinaka, T. D. Matsuda, Y. Aoki, N. L. Saini, and T. Mizokawa, Phys. Rev. B **94**, 081106(R) (2016).

36) A. Nishida, H. Nishiate, C. Lee, O. Miura, and Y. Mizuguchi, J. Phys. Soc. Jpn. 85, 074702 (2016).

37) J. Liu, D. Fang, Z. Wang, J. Xing, Z. Du, X. Zhu, H. Yang, and H.-H. Wen, Europhys.

Lett. 106, 67002 (2014).
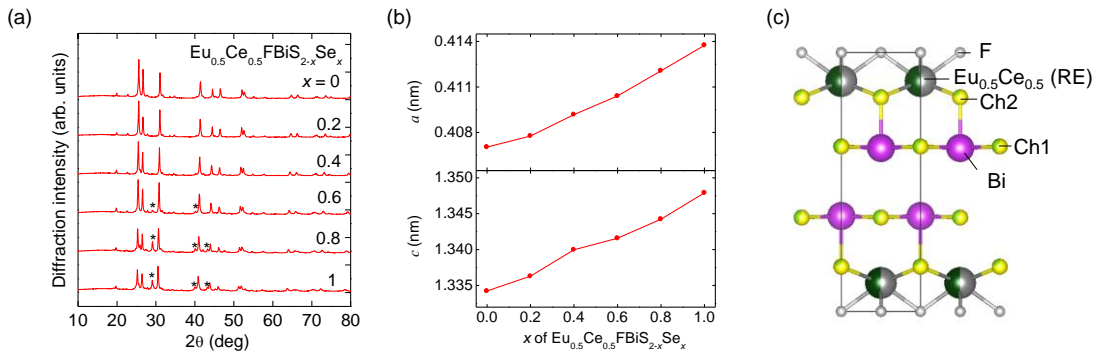
**Figure 1.** (a) XRD patterns of $Eu_{0.5}Ce_{0.5}FBiS_{2-x}Se_x$ for $x = 0-1$. Asterisks denote the diffraction due to Bi_2Se_3 impurity phase. Rietveld fitting patterns were shown in Supplemental Materials. (b) Lattice constants versus x for $Eu_{0.5}Ce_{0.5}FBiS_{2-x}Se_x$. (c) Schematic representation of crystal structure for $x = 0.6$ as a representative sample.
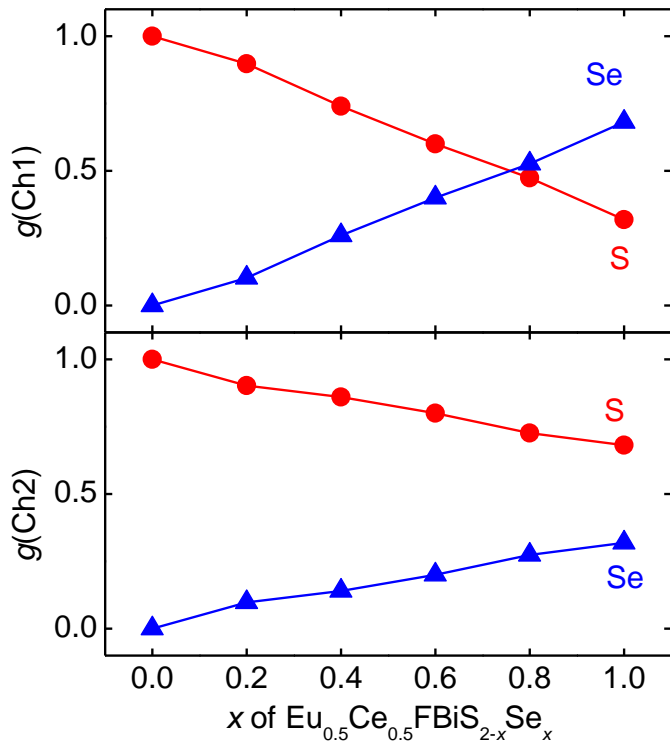
Figure 2. Site occupancies (g) of in-plane Ch1 and out-of-plane Ch2 sites for $Eu_{0.5}Ce_{0.5}FBiS_{2-x}Se_x$.
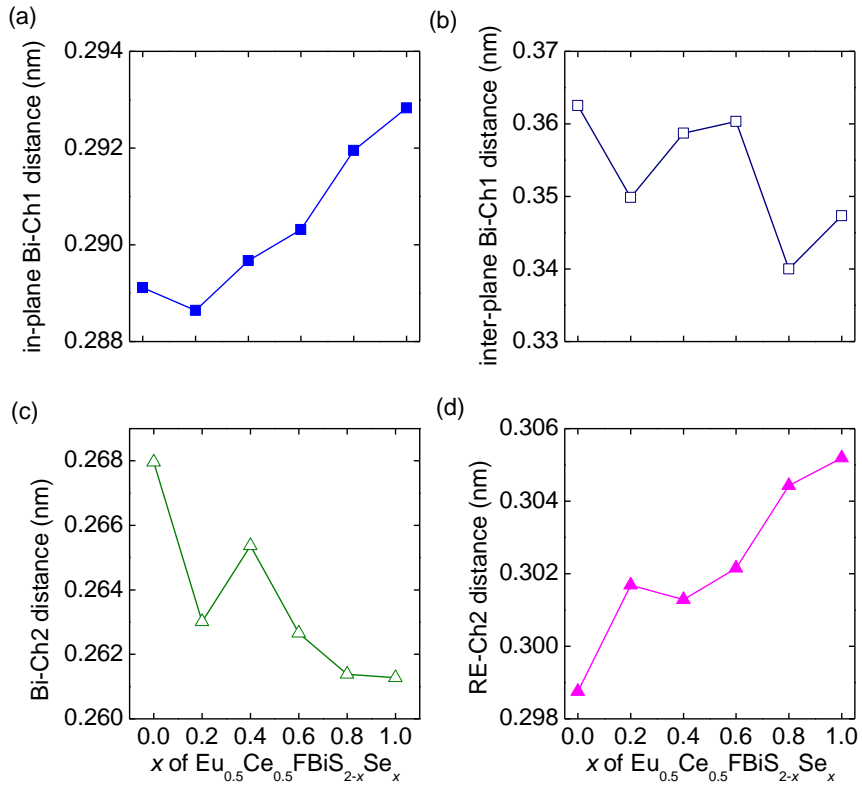
Figure 3. Se concentration dependences of selected bond distances for $Eu_{0.5}Ce_{0.5}FBiS_{2-x}Se_x$: (a) in-plane Bi-Ch1 distance, (b) inter-plane Bi-Ch1 distance, (c) Bi-Ch2 distance, and (d) RE-Ch2 distance.
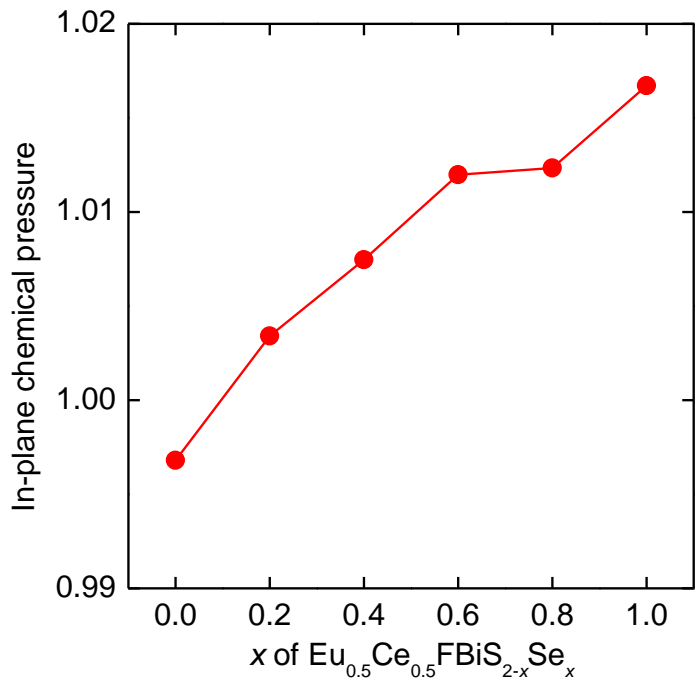
**Figure 4.** In-plane chemical pressure as a function of Se content for $Eu_{0.5}Ce_{0.5}FBiS_{2-x}Se_x$.
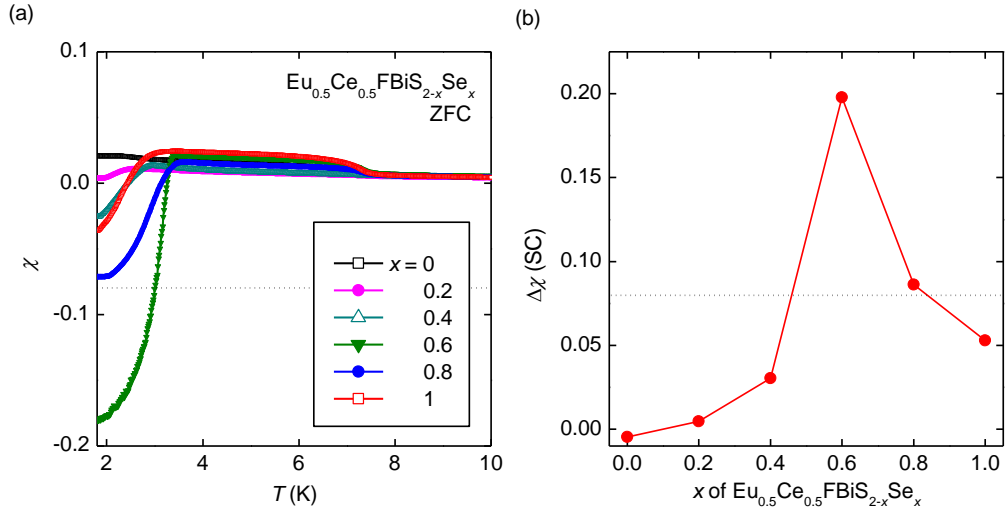
Figure 5. (a) Temperature (T) dependences of magnetic susceptibility (χ) for Eu$_{0.5}$Ce$_{0.5}$FBiS$_{2-x}$Se$_x$ measured after zero-field cooling (ZFC). Dashed line represents the shielding fraction corresponding to -1/4π. χ–T plots after field cooling (FC) were shown in Figure S2. (b) Diamagnetic signal due to superconductivity ($\Delta\chi$(SC)) for Eu$_{0.5}$Ce$_{0.5}$FBiS$_{2-x}$Se$_x$. $\Delta\chi$(SC) was evaluated from the difference of χ between 4 K and 2 K.
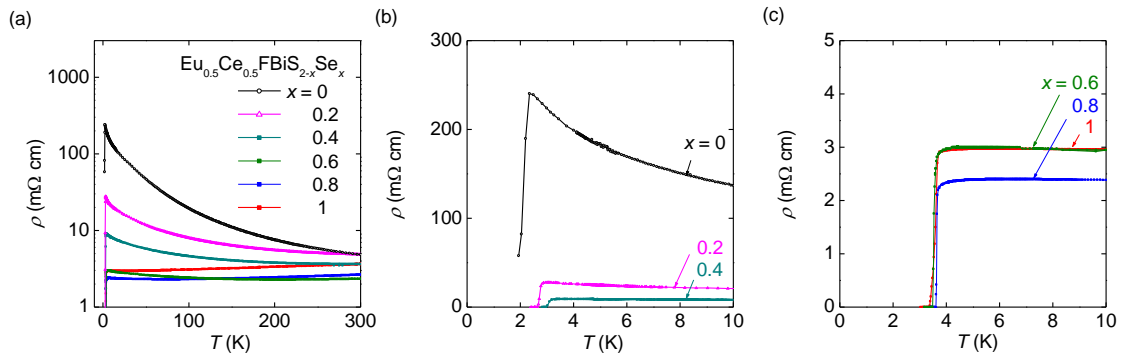
Figure 6. (a) Temperature (T) dependences of electrical resistivity (ρ) for Eu$_{0.5}$Ce$_{0.5}$FBiS$_{2-x}$Se$_x$. (b, c) ρ–T plots below 10 K.
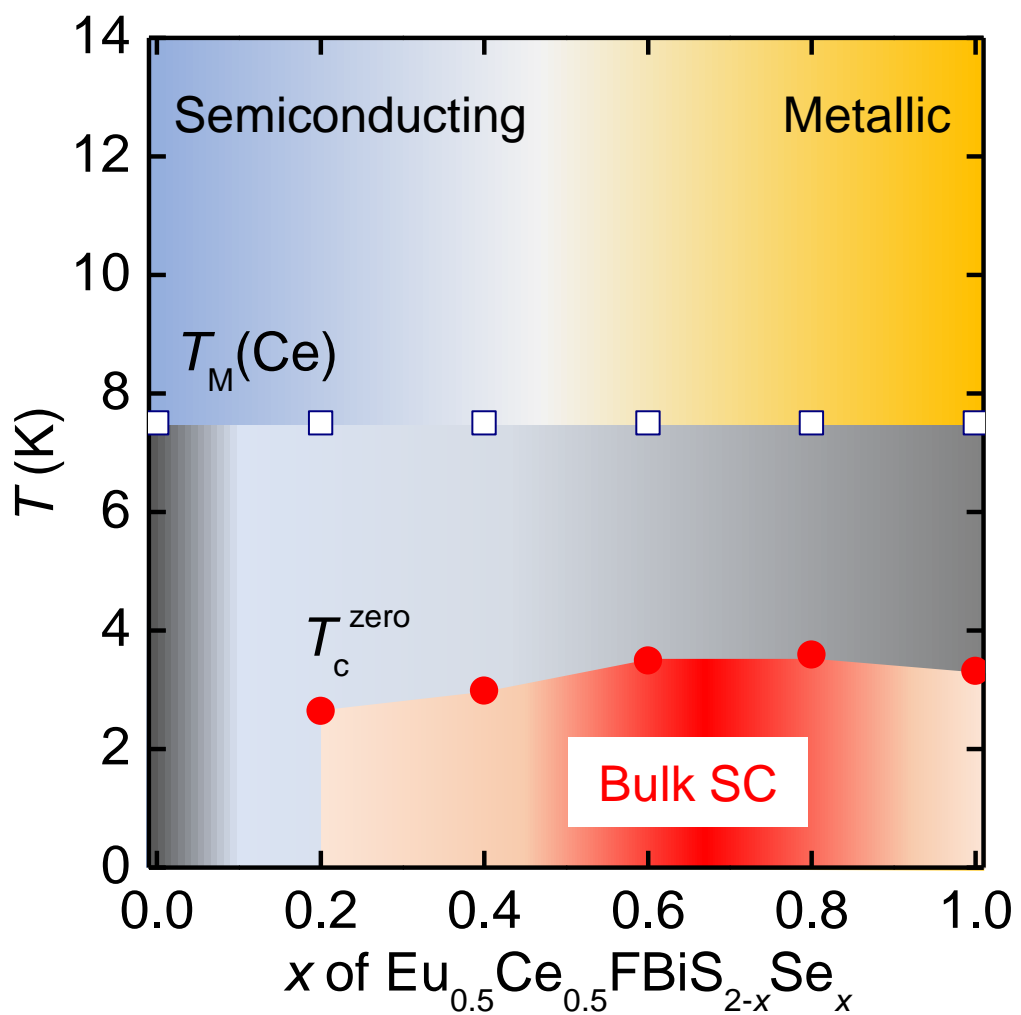
Figure 7. Superconductivity phase diagram of $Eu_{0.5}Ce_{0.5}FBiS_{2-x}Se_x$. T_c^{zero} estimated from the ρ–T data were plotted for $x = 0.2$–1. SC denotes superconductivity.
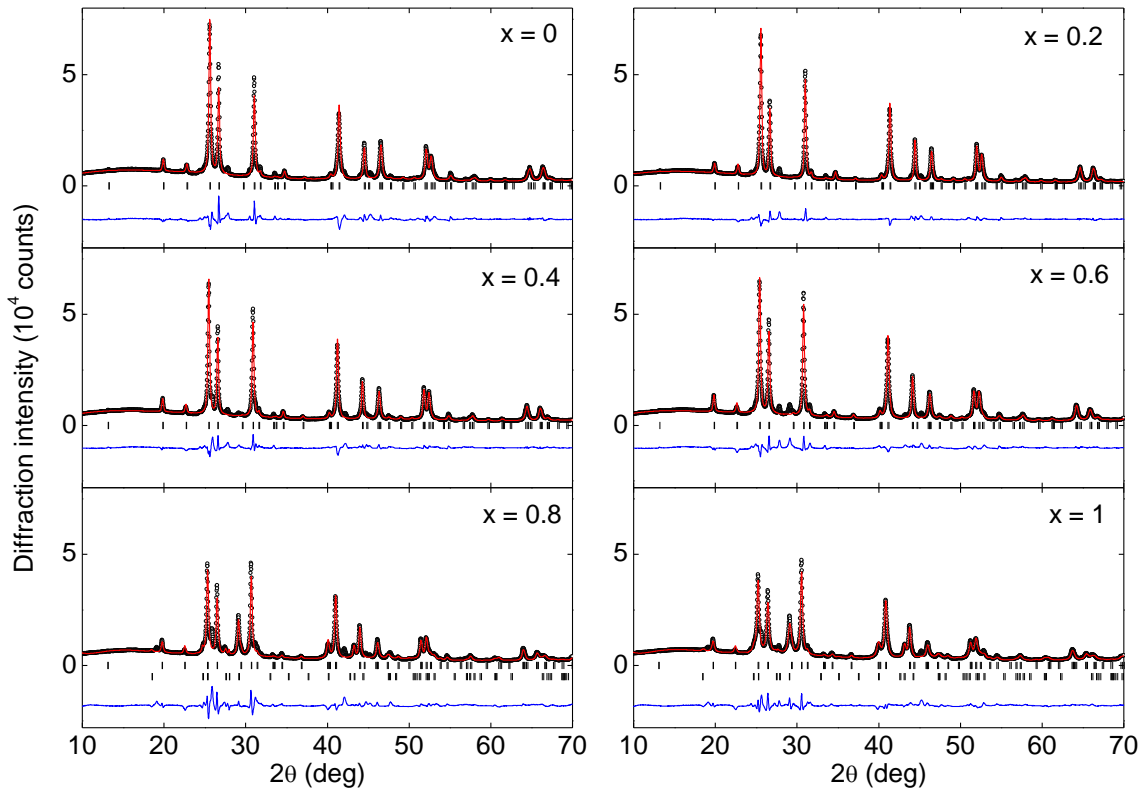
**Figure S1.** XRD patterns and Rietveld refinements of $Eu_{0.5}Ce_{0.5}FBiS_{2-x}Se_x$. For = 0.8 and 1, Bi_2Se_3 was included as a secondary phase. Bragg diffraction angles of Bi_2Se_3 were denoted in lower tick marks.
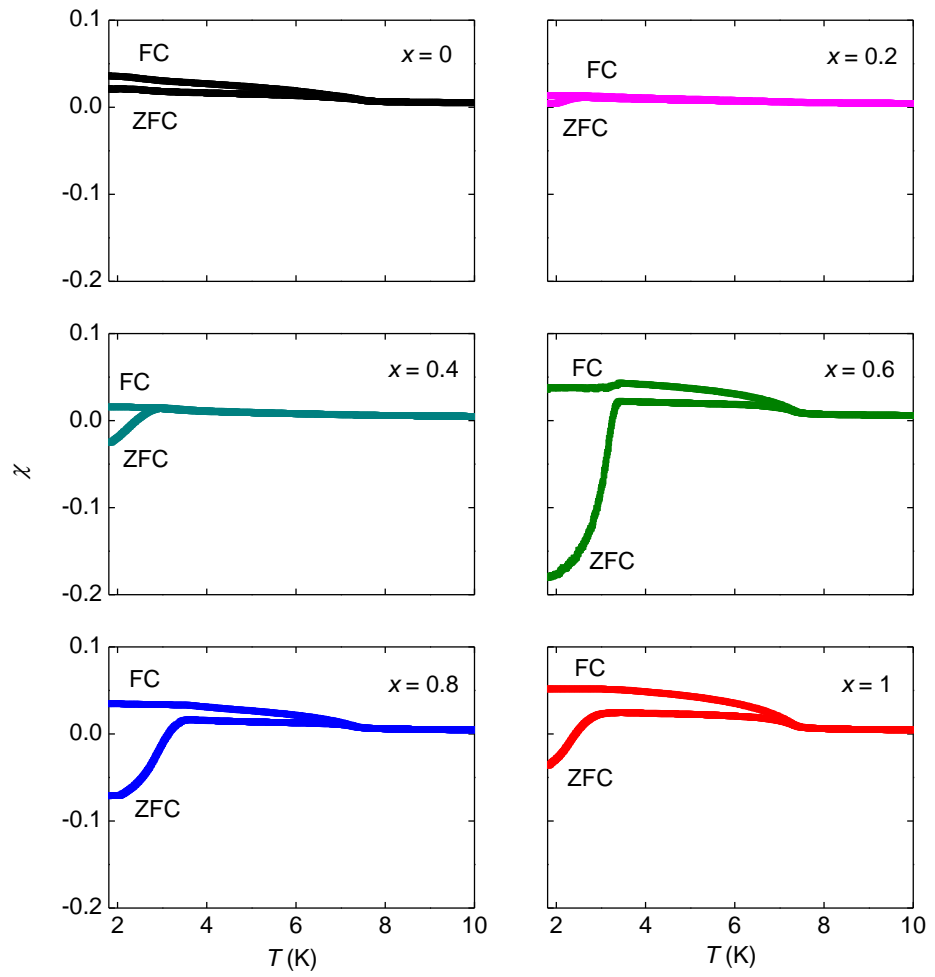
**Figure S2.** Temperature (T) dependences of magnetic susceptibility (χ) for Eu$_{0.5}$Ce$_{0.5}$FBiS$_{2-x}$Se$_x$ measured after zero-field cooling (ZFC) and field cooling (FC). An gradual increase of χ below 8 K was most likely due to ferromagnetic order of Ce^{3+} ions.